SUPPORTING INFORMATION

Kinetic and Structural Insights into the Mechanism of Binding of Sulfonamides to Human Carbonic Anhydrase by Computational and Experimental Studies

Roberto Gaspari,[†] Chris Rechlin,[‡] Andreas Heine,[‡] Giovanni Bottegoni,[†] Walter Rocchia,[†] Daniel Schwarz,[§] Jörg Bomke,[§] Hans-Dieter Gerber,[‡] Gerhard Klebe,[,‡] Andrea Cavalli,[*,†,||]*

[†]Department of Drug Discovery and Development, Istituto Italiano di Tecnologia, 16163 Genova, Italy

[‡]Department of Pharmaceutical Chemistry, Philipps-University Marburg, Marbacher Weg 6, 35032 Marburg, Germany

[§]Merck KGaA, Merck Serono Research, Small Molecule Platform/MIB, Frankfurter Str. 250, 64293 Darmstadt, Germany

[||]Department of Pharmacy and Biotechnology, University of Bologna, 40126 Bologna, Italy

[*]To whom correspondence should be addressed: GK, Klebe@Staff.Uni-Marburg.de; AC, Andrea.Cavalli@iit.it

Table of contents

SECTION A. EXPERIMENTAL DETAILS.

Details of ligand verification and purification.

All tested compounds were commercially obtained. Except for **5,** their identity as well as purity of at least 95 % or higher was verified by the methods described below. Melting points were determined on a Leitz HM-Lux melting point microscope and are uncorrected. Proton NMR spectra were recorded on a JEOL ECA-500 MHz spectrometer (^{1}H NMR: 500.2 MHz) or a JEOL ECX-400 MHz spectrometer (^{1}H NMR: 399.8 MHz). Quantitative NMR (qNMR) measurements[1, 2] regarding compound **5** were exclusively performed at 500.2 MHz. As Certified Reference Material (CRM), maleic acid (δ 6.26 ppm), purchased from Sigma Aldrich, was used as internal reference standard. Chemical shifts are stated in parts per million (ppm) and were referenced to tetramethylsilane (TMS) at δ 0.00 ppm, except for qNMR measurements, where the solvent residual peak for DMSO-d_6 at δ 2.50 ppm served as reference. qNMR purities for the different purity levels of compound **5** were obtained from the calculation of the observed integral values of the CRM and the aromatic 2`,6` protons in relation to their molar proportion to each other using the formula described below.[1] NMR instrument parameters were in accordance with those required for standard qNMR measurements.[2] The NMR data were processed employing Delta NMR Processing and Control Software, version 5.0.0. Abbreviations concerning signal multiplicity are as follows: bs = broad singlet, d = doublet, m = multiplet, q = quartet, s = singlet, sext = sextet, t = triplet.

ESI+ mass spectra were obtained from a Q-trap 2000 triple quadrupol mass spectrometer (Applied Biosystems). Elemental combustion analyses were determined on a vario Micro cube CHNS analyzer (Elementar Analysensysteme GmbH). Chromatography was performed using prepacked silica gel columns (Interchim PuriFlash SI-HP, 30 μm). TLC was carried out using 0.2 mm aluminium plates coated with silica gel 60 F_{254} (Macherey-Nagel) and the respective substance

spots were visualized by UV detection. Solvents for chromatography of compound **5** were used in analytical quality without further purification.

ligands 1-5:

benzenesulfonamide (**1**)[3-5]. Mp: 151-153 °C(lit.[4]: 155-158 °C); ^{1}H NMR (500.2 MHz, [D$_6$]DMSO): δ = 7.85-7.82 (m, 2H), 7.61-7.54 (m, 3H), 7.32 (br s, 2H). MS (ES+) *m/z* 175 [M + NH$_4$]$^+$. Elemental analysis calculated (%) for $C_6H_7NO_2S$: C 45.85, H 4.49, N 8.91. Found: C 45.30, H 4.43, N 9.02.

4-methylbenzene-1-sulfonamide (**2**)[3-5]. Mp: 137-139 °C(lit.[3]: 136 °C); ^{1}H NMR (399.8 MHz, [D$_6$]DMSO): δ = 7.71 (d, ^3J(H,H) = 8.2 Hz, 2H), 7.36 (d, ^3J(H,H) = 8.2 Hz, 2H), 7.25 (br s, 2H), 2.37 (s, 3H). MS (ES+): *m/z* 189 [M + NH$_4$]$^+$. Elemental analysis calculated (%) for $C_7H_9NO_2S$: C 49.11, H 5.30, N 8.18. Found: C 48.97, H 5.27, N 8.13.

4-ethylbenzene-1-sulfonamide (**3**)[6]. Mp: 110-111 °C(lit.[6]: 109-111 °C); ^{1}H NMR (500.2 MHz, [D$_6$]DMSO): δ = 7.73 (d, ^3J(H,H) = 8.3 Hz, 2H), 7.39 (d, ^3J(H,H) = 8.3 Hz, 2H), 7.23 (br s, 2H), 2.67 (q, ^3J(H,H) = 7.7 Hz, 2H); 1.19 (t, ^3J(H,H) = 7.7 Hz, 3H). MS (ES+) *m/z* 203 [M + NH$_4$]$^+$. Elemental analysis calculated (%) for $C_8H_{11}NO_2S$: C 51.87, H 5.99, N 7.56. Found: C 51.86, H 5.94, N 7.72.

4-propylbenzene-1-sulfonamide (**4**)[7]. Mp: 101-105 °C(lit.[7]: 98-101 °C) ^{1}H NMR (399.8 MHz, [D$_6$]DMSO): δ = 7.73 (d, ^3J(H,H) = 8.2 Hz, 2H), 7.37 (d, ^3J(H,H) = 8.2 Hz, 2H), 7.25 (br s, 2H), 2.62 (t, ^3J(H,H) = 7.6 Hz, 2H); 1.61 (sext, ^3J(H,H) = 7.6 Hz, 2H), 0.89 (t, ^3J(H,H) = 7.3 Hz, 2H). MS (ES+) *m/z* 217 [M + NH$_4$]$^+$. Elemental analysis calculated (%) for $C_9H_{13}NO_2S$: C 54.27, H 6.58, N 7.03. Found: C 53.81, H 6.55, N 7.21.

4-(2-hydroxyethyl)-benzene-1-sulfonamide (5)[8]: The commercial compound was chromatographed twice on a prepacked silica gel column utilizing chloroform:ethyl acetate, 10:1 (v/v) as eluent. Mp: 85-88 °C(lit.[8]: 54-55 °C). TLC ($CHCl_3$: EtOAc 10 : 1): R_f = 0.13. ^{1}H NMR (500.2 MHz, [D$_6$]DMSO): δ = 7.72 (d, ^3J(H,H) = 8.3 Hz, 2H), 7.40 (d, 2H, J = 8.3 Hz), 7.24 (br s, 2H), 4.68 (br t, 1H) 3.63 (m, 2H) 2.79 (t, ^3J(H,H) = 6.7 Hz, 2H). MS (ES+) *m/z* 219 [M + NH$_4$]$^+$.

Elemental analysis calculated (%) for $C_8H_{11}NO_3S$: C 47.75, H 5.51, N 6.96. Found: C 47.69, H 5.67, N 6.88.

reference ligands 6 and 7:

4-carbonyloxybenzene-1-sulfonamide (4-sulfamoylbenzoic acid) (6)[9, 10]. Mp: 276-277 °C (lit.[9]: 282-283 °C); ^{1}H NMR (500.2 MHz, [D$_6$]DMSO): δ = 13.33 (br s, 1H), 8.11 (d, ^3J(H,H) = 8.6 Hz, 2H), 7.94 (d, ^3J(H,H) = 8.6 Hz, 2H), 7.51 (br s, 2H); MS (ES-) *m/z* 200 [M - H]$^-$. Elemental analysis calculated (%) for $C_7H_7NO_4S$: C 41.79, H 3.51, N 7.03. Found: C 42.14, H 3.66, N 7.13

4-aminobenzene-1-sulfonamide (sulfanilamide) (7)[11]. Mp: 165-167°C(lit.[11]: 163-165 °C); ^{1}H NMR (500.2 MHz, [D$_6$]DMSO): δ = 7.45 (d, ^3J(H,H) = 8.9 Hz, 2H), 6.58 (d, ^3J(H,H) = 8.9 Hz, 2H)), 5.76 (br s, 2H). MS (ES+) *m/z* 190 [M + NH$_4$]$^+$. Elemental analysis calculated (%) for $C_9H_{13}NO_2S$: C 41.85, H 4.68, N 16.26. Found: C 41.86, H 4.69, N 16.29.

Calculation of the purity (**P**) of the sample (analyte) **5** according to qNMR measurements was performed by the following formula: lit.[1]

$$P = \frac{I_{analyte}}{I_{CRM}} x \frac{N_{CRM}}{N_{analyte}} x \frac{M_{analyte}}{M_{CRM}} x \frac{m_{CRM}}{m_{sample}} \quad x\, P_{CRM}$$

P = purity of sample (%)
$I_{analyte}$ = integral of analyte signal
N_{CRM} = number of CRM protons
$M_{analyte}$ = molecular mass of analyte
m_{CRM} = mass of CRM
I_{CRM} = integral of CRM signal
$N_{analyte}$ = number of analyte protons
M_{CRM} = molecular mass of CRM
m_{sample} = mass of sample/analyte
P_{CRM} = purity of CRM (%)

qNMR data of commercial **5**:
(**$I_{analyte}$**) of **5**: 1.61

(N_{CRM}) of CRM 2
($M_{analyte}$) of **5**: 201.24 g/mol
(m_{CRM}) of CRM: 4.22 mg
(I_{CRM}) of CRM. 2.00
($N_{analyte}$) of **5**: 2
(M_{CRM}) of CRM: 116.07 g/mol
(m_{sample}) of **5**: 6.93 mg
(P_{CRM}) of CRM: 100 %

purity (**P**) of commercial **5** in %:

$$P = I_{analyte} * N_{CRM} * M_{analyte} * m_{CRM} * p_{CRM} / I_{CRM} * N_{analyte} * M_{CRM} * m_{sample}$$

P = 1.61* 2 * 201.24 g/mol * 4.22 mg * 100 % / 2.00 * 2 * 116.07 g/mol * 6.93 mg

= **84.99 %**

qNMR data of chromatographed **5** (1. purification step):
($I_{analyte}$) of **5**: 1.84
(N_{CRM}) of CRM 2
($M_{analyte}$) of **5**: 201.24 g/mol
(m_{CRM}) of CRM: 4.16 mg
(I_{CRM}) of CRM: 2.00
($N_{analyte}$) of **5**: 2
(M_{CRM}) CRM: 116.07 g/mol
(m_{sample}) of **5**: 7.04 mg
(P_{CRM}) of CRM: 100 %

purity (**P**) of chromatographed **5** in % (1. purification step):

P = 1.84 * 2 * 201.24 g/mol * 4.16 mg * 100 % / 2.00 * 2 * 116.07 g/mol * 7.04 mg

= **94.25 %**

qNMR data of chromatographed **5** (2. purification step):
($I_{analyte}$) of **5**: 2.07
(N_{CRM}) of CRM 2
($M_{analyte}$) of **5**: 201.24 g/mol
(m_{CRM}) of CRM: 4.07 mg
(I_{CRM}) of CRM. 2.00
($N_{analyte}$) **5**: 2
(M_{CRM}) of CRM: 116.07 g/mol
(m_{sample}) of **5**: 7.48 mg
(P_{CRM}) of CRM: 100 %

purity (**P**) of chromatographed **5** in % (2. purification step):

P = 2.07 * 2 * 201.24 g/mol * 4.07 mg * 100 % / 2.00 * 2 * 116.07 g/mol * 7.48 mg

= **97.64 %**

SECTION B. SUPPORTING FIGURES.

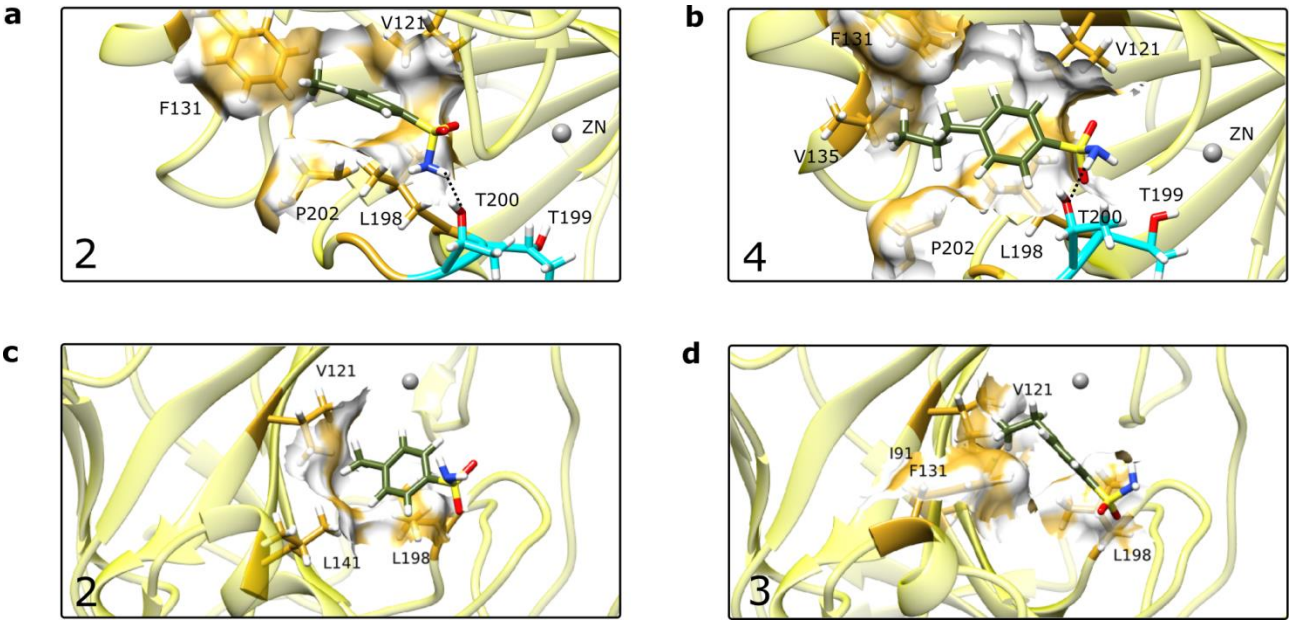

Figure S1. Conformational clustering of MD trajectories. (a,b) Most populated S conformations found in plain MD for ligands **2** and **4**. (c,d) Most populated F conformations found in plain MD for ligands **2** and **3**.

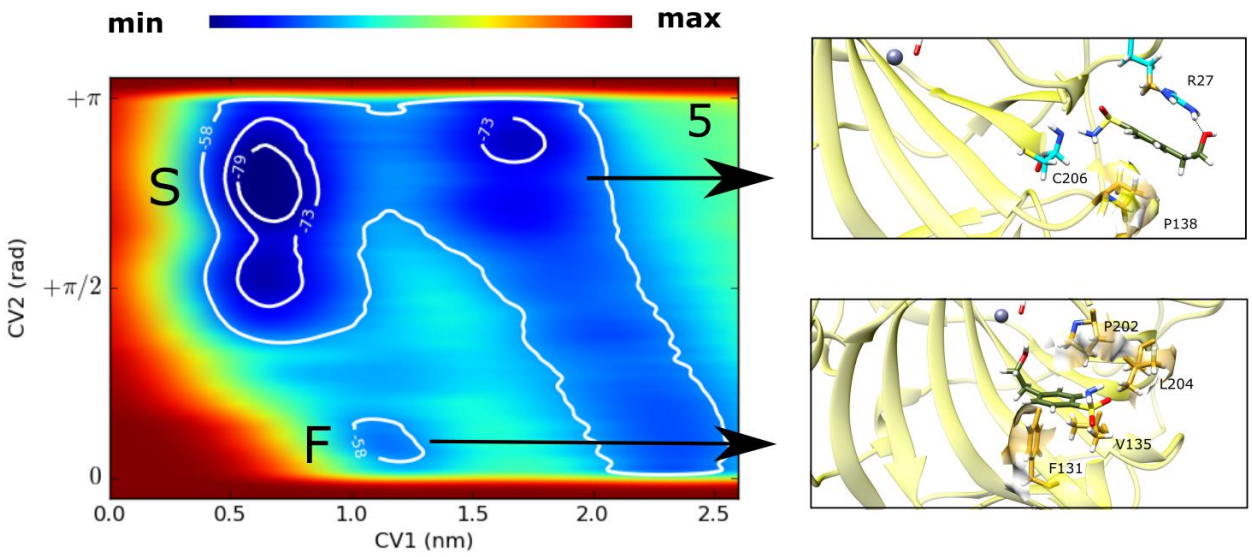

Figure S2. Conformations in the secondary free energy minima of ligand **5**. Figure explanation follows the caption of Figure 3.

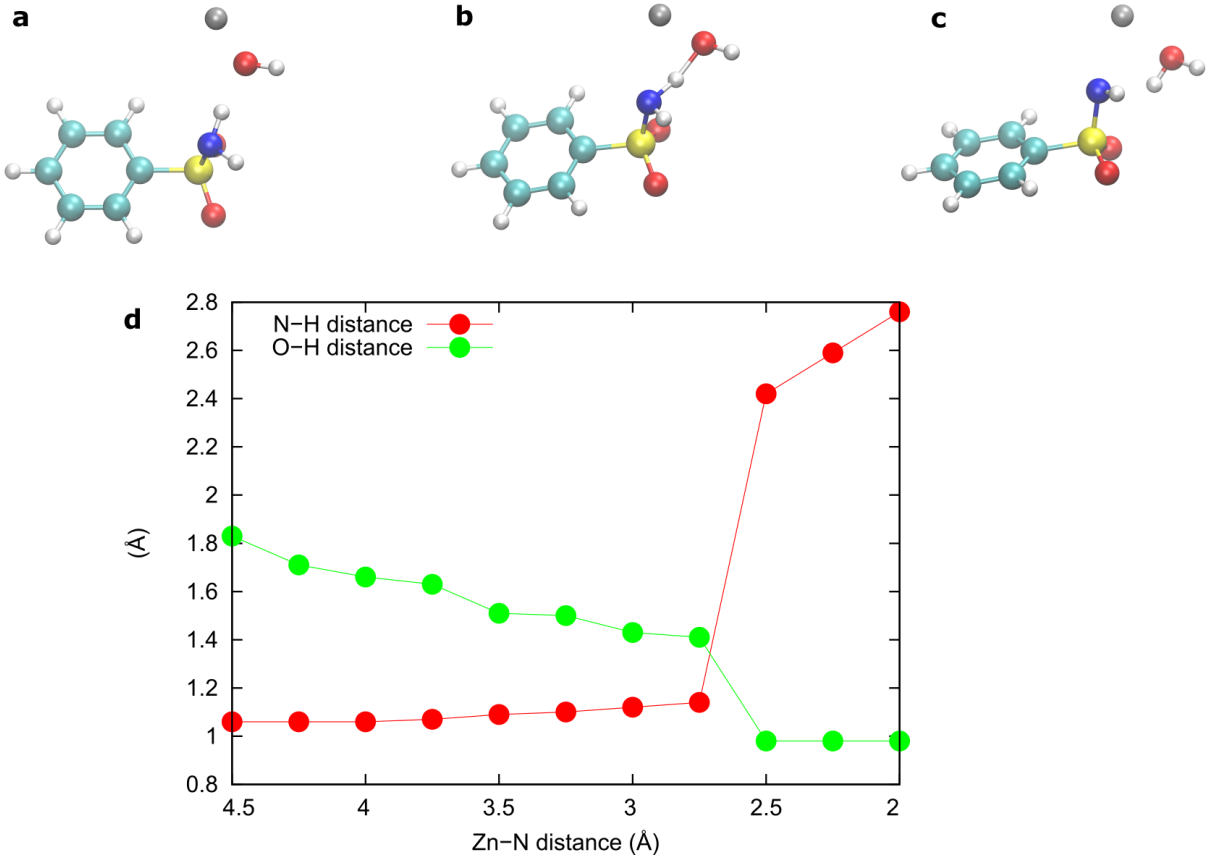

Figure S3. Sulfonamide-hydroxyl proton transfer. (a,b,c) Subset of the system used for the constrained geometry optimizations. The benzenesulfonamide, the hydroxyl ion (or water molecule) and the zinc ion are reported. The images depict the optimized geometry at a Zn-N distance of 3.50 (a), 2.75 (b) and 2.50 Å (c). (d) The length of the N-H bond in the sulfonamide as well as the O-H distance between the hydroxyl oxygen and the incoming proton are reported as a function of the Zn-N distance.

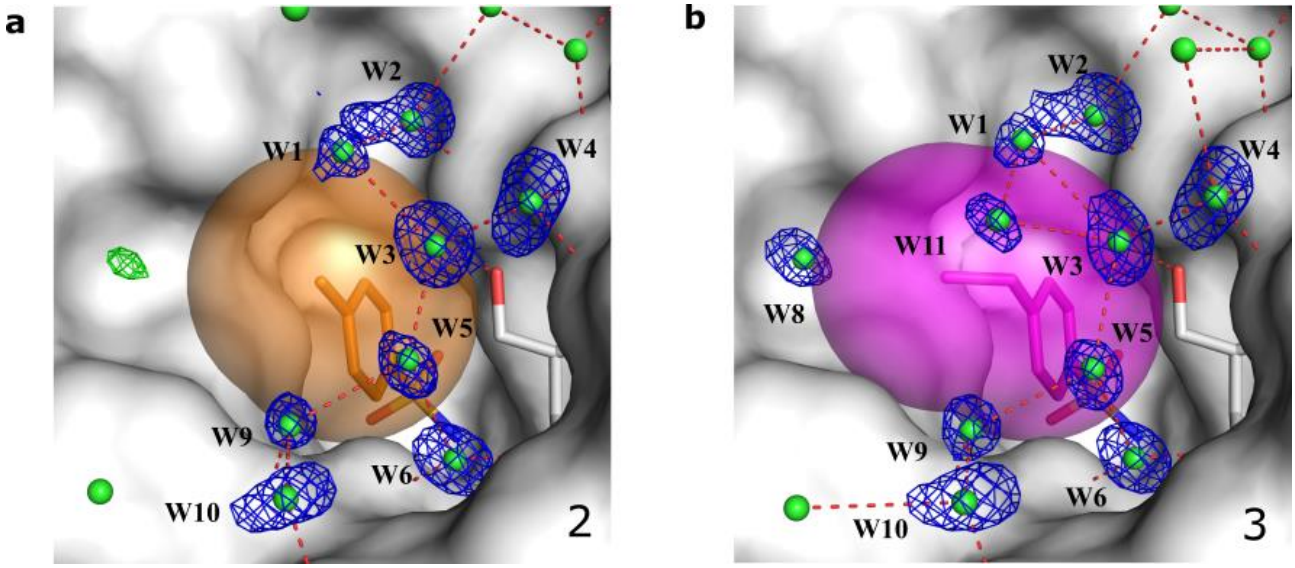

Figure S4. Crystallographic structure of ligands **2** and **3** in the Zn^{2+}-bound conformation. (a) ligand **2,** (b) ligand **3**. Figure explanation follows the caption of Figure S5. The $2F_o$-F_c densities are shown at a sigma level of 0.9 σ (hCAII-**2**) and 1.0 σ (hCAII-**3**), respectively. For hCAII-**2** (a) at the position of W8, the observed F_o-F_c difference electron density is shown (3.13 σ , 0.50 e/Å^3) indicating some occupancy of a water molecule at this site.

.

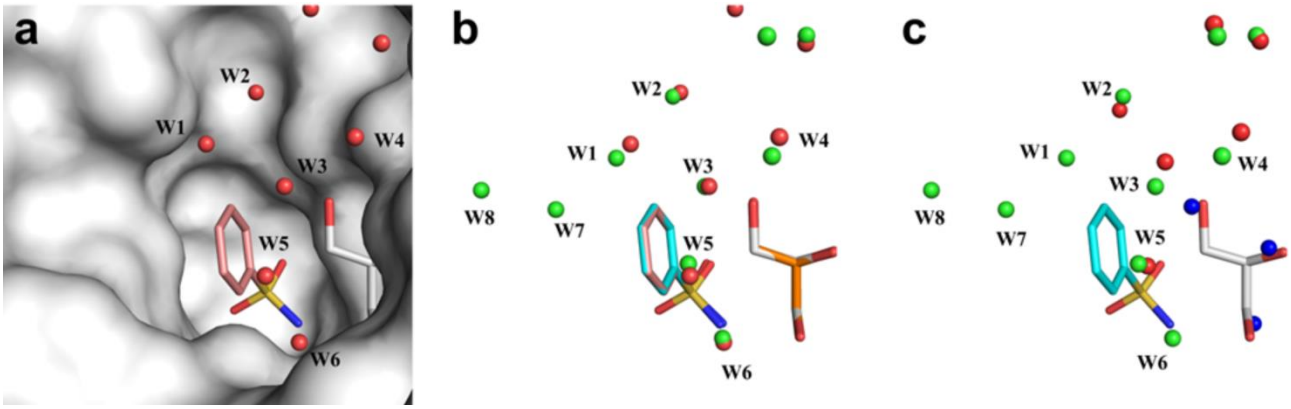

Figure S5. Comparison between ligand **1** and the previously published 2WEJ structure. (a) Previously published crystal structure of **1** complexed to hCAII (1.45 Å, pdb: 2WEJ[12]). Oxygen atoms are colored in red, sulfur atoms in yellow and nitrogen atoms in blue. Carbon atoms of **1** are colored in salmon. (b) Alignment of the hCAII-**1** structure which is reported in this work (1.01 Å) with the structure with the pdb-code 2WEJ. The carbon atoms of **1** of the here reported hCAII-1 structure are shown in cyan. The positions of **1**, glycerol and the water molecules W1-W6 align very well. Two additional waters (W7, W8) can be placed in the difference density in our structure. Presumably, they were not detected in the previous structure due to the lower resolution.(c) Comparison of the water structures in complexes of the hCAII-**1** and of the *apo*-protein (pdb: 3KS3[13]). The water molecules in hCAII-**1** are shown as green spheres. The carbon atoms of the glycerol molecule which is present in all hCAII-**1** complexes are shown in grey, the carbon atoms of **1** are shown in cyan. The water molecules of the *apo*-structure which are displaced by the glycerol molecule are shown as blue spheres, the water molecules of the *apo*-structure which are also present in the hCAII-**1** structure are shown in red.

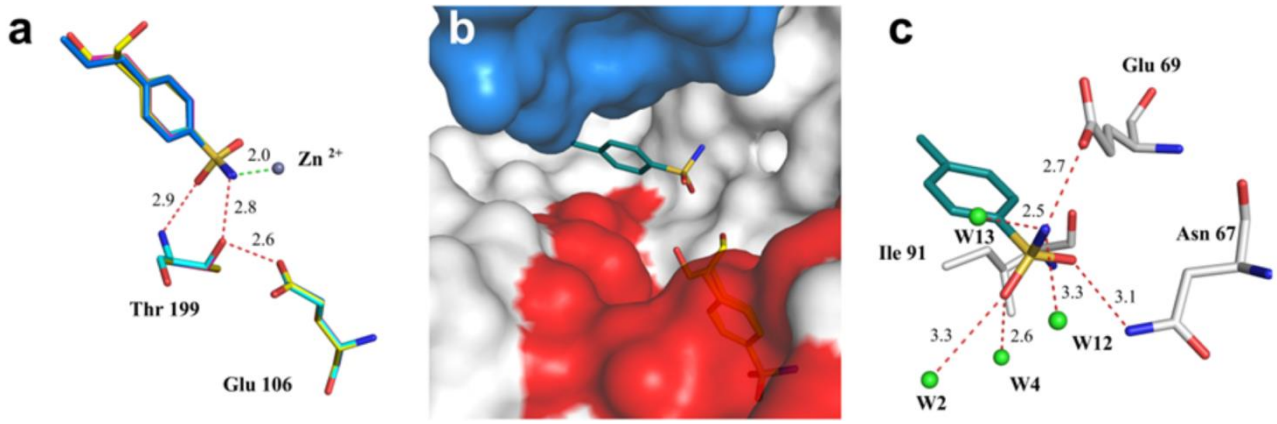

Figure S6. Additional details of the crystallographic binding modes of 5. (a) Alignment of crystal structures hCAII-**1** – hCAII-**5**. Oxygen atoms are colored in red, sulfur atoms in yellow and nitrogen atoms in blue. The zinc ion is shown as a gray sphere. H-bond distances are shown as red-dotted lines. The distance between the zinc ion and the nitrogen of the ligands is shown as a green-dotted line. Carbon atoms of the ligand and of the corresponding protein residues are colored in green for **1**, in orange for **2**, in purple for **3**, in light-blue for **4** and in yellow for **5**. The binding modes of **1**-**5** align nearly perfectly. (b) The binding positions of **5** in the active site and at the surface next to the hydrophobic patch are shown. The surface of hCAII is colored in gray, the residues which form the hydrophobic patch are colored in red. The surface of the hCAII molecule of the next symmetry mate is colored in blue. One molecule of **5** binds as expected deeply buried in the active site (carbon atoms are colored in yellow). A second molecule of **5** binds additionally at the entrance of the binding pocket with contacts to the hydrophobic patch (carbon atoms are colored in turquoise). Only the first carbon atom of the hydroxyethylene tail of **5** was modeled into the density since the remaining atoms were not well defined in the difference electron density. (c) Interactions of the second molecule of **5**. Carbon atoms of the protein residues of the hCAII are shown in gray. Water molecules are shown as green spheres.

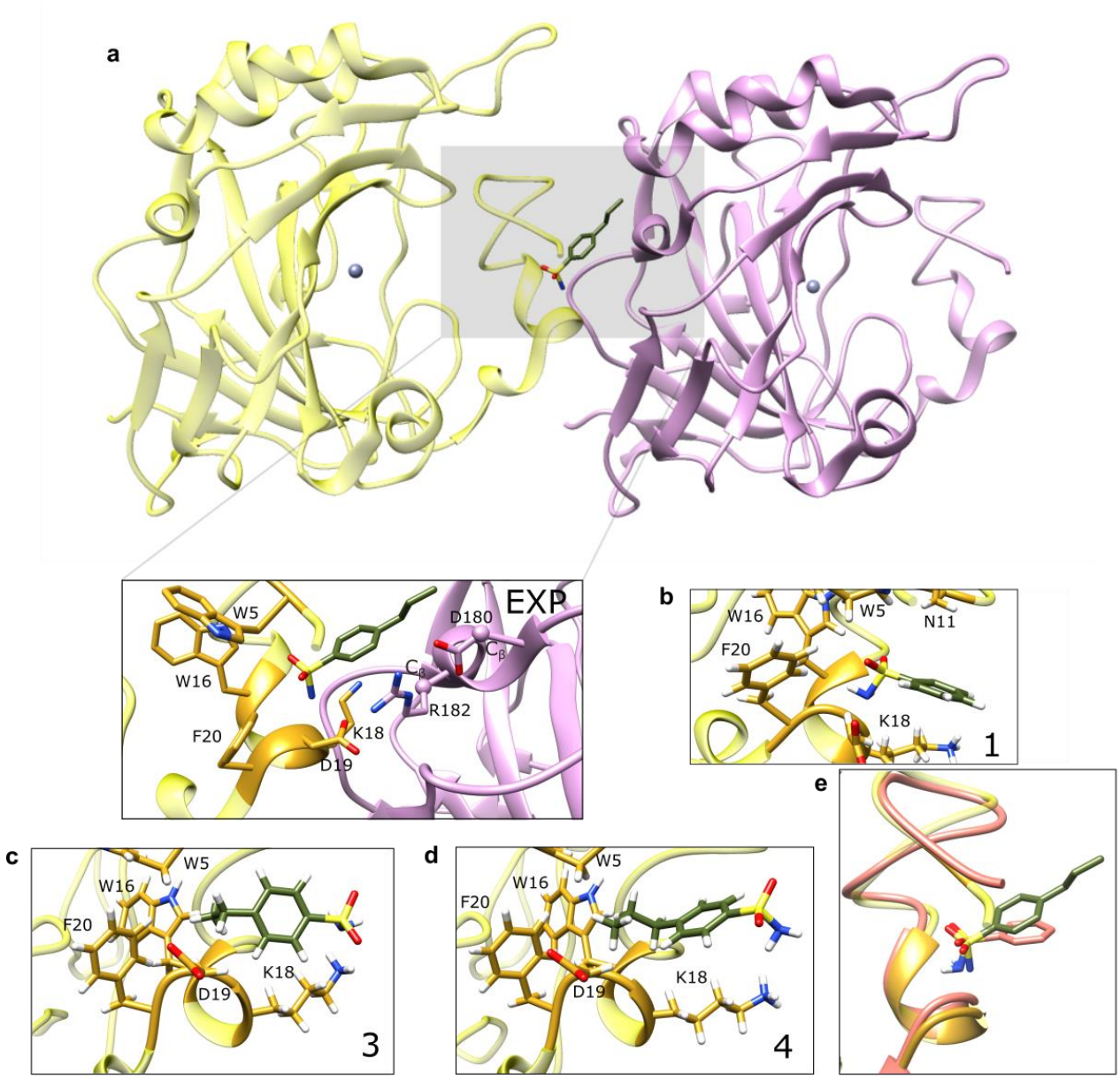

Figure S7. Binding modes at the N-terminal cleft. (a) Structural overview of the crystallographic protein-ligand system. The ligand **4** is shown together with the two proteins (colored yellow and violet, respectively) with which it forms contacts. In the inset we show the residues whose distance from the ligand is less than 4 Å. The ligand forms interactions with the N-terminus cleft of the first protein (yellow) and the C_β of D180 and R182 (minimum C_β-C) of the second protein (violet).The minimum distance between the C_β and the sulfonamide carbons is 4.1 Å (R182) and 4.0 Å (D180). (b,c,d) Center of conformational clusters obtained by simulations. (b) ligand **1** (population = 0.6%) (c) ligand **3** (population = 5%) (d) ligand **4** (population = 6%) (e) Alignment at the N-terminus between the crystallography structure and the

configuration reported in (b). The structures of ligand **4** and **5** in the N-terminal cleft were found predominantly with the polar sulfonamide pointing outwards, at variance with the experimental result. The crystallographic structure could not be recapitulated presumably because of the unfavorable interaction between the larger alkyl tail and the surrounding water. This interaction is on the other hand lifted in the crystal structure by the protein packing, thereby providing an explanation for the observed behavior.

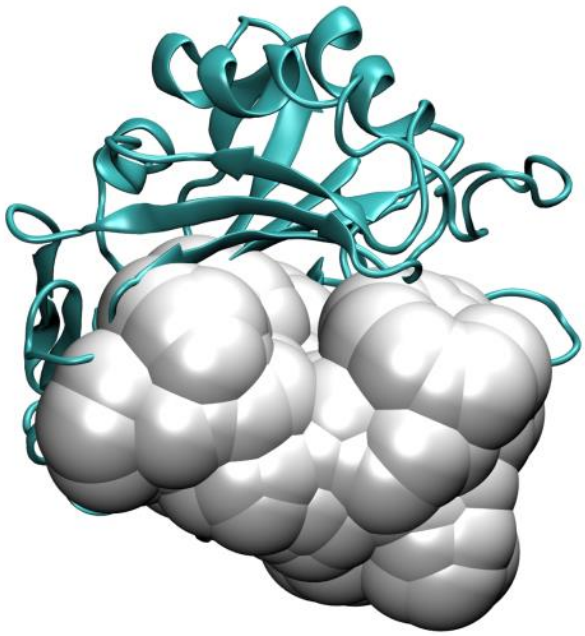

Figure S8. Confining region of ligands in simulations. Confining region, represented as a union of spheres (white balloons), overlaid on a cartoon representation of hCAII.

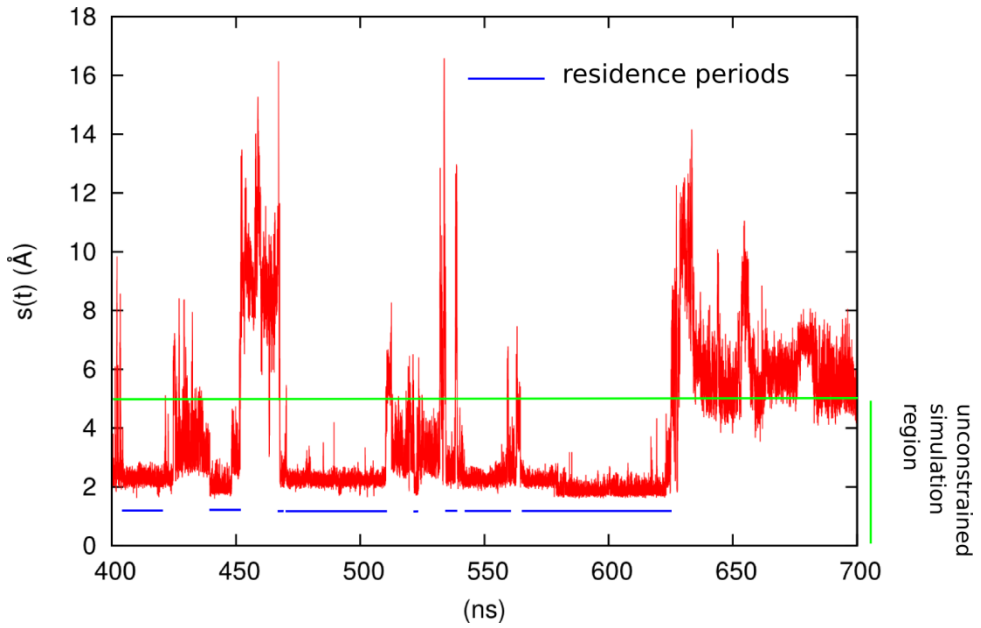

Figure S9. Example of residence time determination. The minimum distance s(t) between the ligand and the HP patch is plotted during part of the trajectory of hCAII-**3** system. The broken blue line identifies the different residence periods, which are delimited by abrupt spikes of s(t). For values of s(t) larger than the limit depicted by the horizontal green line, a constraining potential favors the repositioning of the ligand on the HP patch, thus enhancing the number of binding/unbinding events in the simulation.

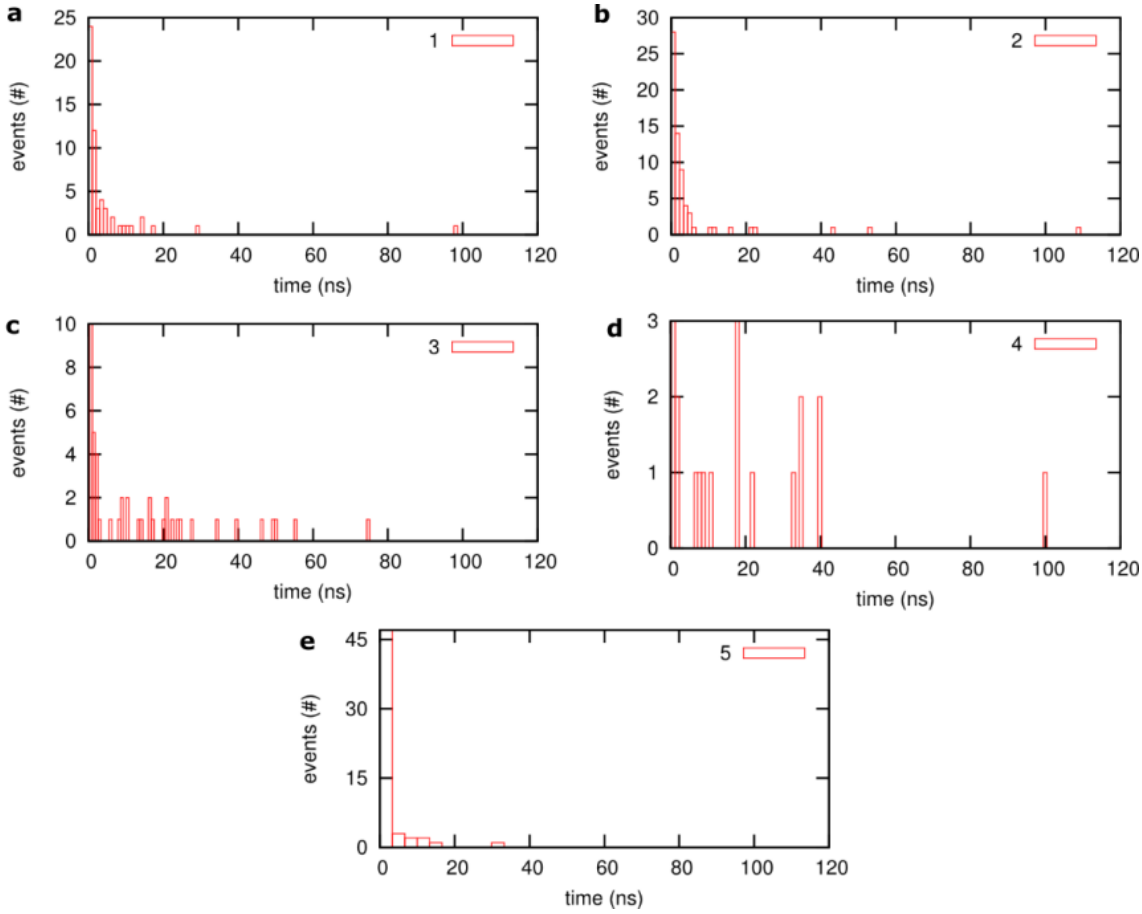

Figure S10. Distribution of the residence times in the HP pocket.**1** (a), **2** (b), **3** (c), **4** (d), **5** (e).

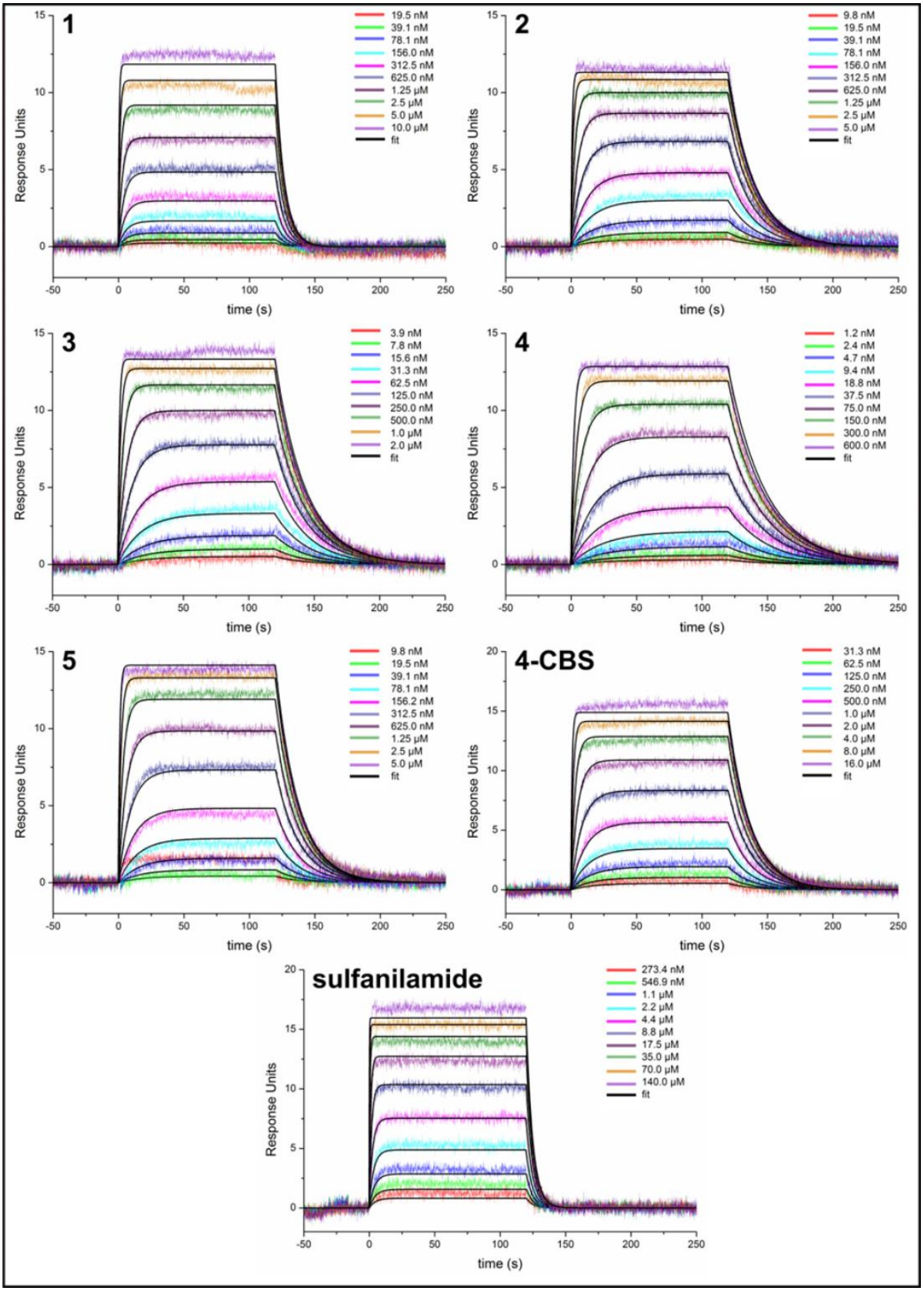

Figure S11. Example curves for the **1**-**5**, 4-CBS (**6**) and sulfanilamide (**7**). The curves for **1**-**5** were measured with a 4900 RU surface, the curves for **6** and **7** with a 4900 RU surface.

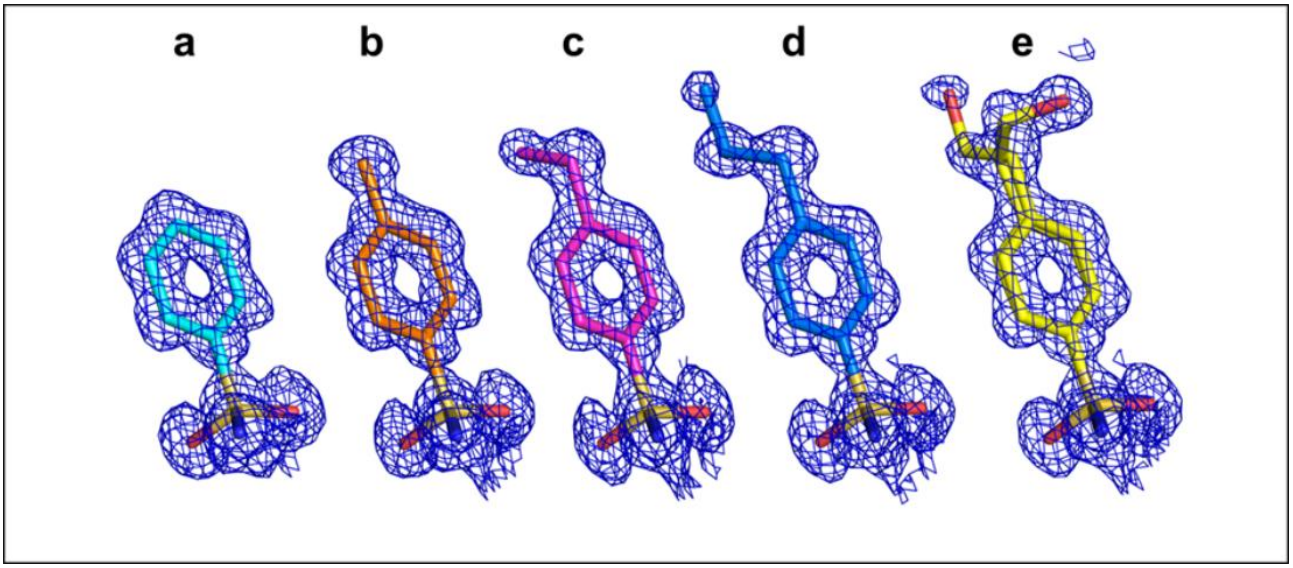

Figure S12. $2F_o$-F_c electron density maps around the bound active site ligands shown as a blue meshes at an iso level of 0.50 electrons/ $Å^3$ for **1** (a, 0.9 σ), **2** (b, 0.9 σ), **3** (c, 1.0 σ), **4** (d, 0.9 σ), and **5** (e, 0.9 σ).

SECTION D. SUPPORTING TABLES.

Lig	Spot 1 (=3700 RU)				Spot 2 (=3600 RU)			
	K_D (st-st) [nM]	K_D (kin) [nM]	k_{on} [x 10^5 1/Ms]	k_{off} [1/s]	K_D (st-st) [nM]	K_D (kin) [nM]	k_{on} [x 10^5 1/Ms]	k_{off} [1/s]
1	1002.0	1073.4	1.6	0.1696	1037.0	1183.9	1.5	0.1828
2	382.2	318.8	1.9	0.0617	429.8	333.5	2.0	0.0664
3	133.7	91.4	5.1	0.0464	157.3	93.8	5.4	0.0504
4	63.4	57.4	8.7	0.0498	66.8	64.5	9.6	0.0617
5	452.8	418.3	1.6	0.0673	488.6	448.0	1.7	0.0741
	Spot 1 (=4900 RU)				**Spot 2 (=4700 RU)**			
	K_D (st-st) [nM]	K_D (kin) [nM]	k_{on} [x 10^5 1/Ms]	k_{off} [1/s]	K_D (st-st) [nM]	K_D (kin) [nM]	k_{on} [x 10^5 1/Ms]	k_{off} [1/s]
1	1076.0	1063.1	1.4	0.1465	1426.0	1278.4	1.2	0.1529
2	218.0	228.8	2.2	0.0498	296.8	290.3	1.9	0.0550
3	104.3	100.3	4.3	0.0426	106.1	107.8	4.2	0.0451
4	53.1	51.4	6.7	0.0345	59.0	57.9	6.2	0.0357
5	358.2	330.3	1.7	0.0567	414.8	371.6	1.6	0.0591

Table S1. Results of the single measurements on four independent protein surfaces for ligands **1-5.** For ligand **5** a sample with a purity of 94% was used. As explained in the experimental part, the results do not significantly differ from the sample with 98% purity.

Ligand	**5 (94%)**				**5 (98%)**			
	K_D (st-st) [nM]	**K_D (kin) [nM]**	**k_{on} [x 10^5 1/Ms]**	**k_{off} [1/s]**	**K_D (st-st) [nM]**	**K_D (kin) [nM]**	**k_{on} [x 10^5 1/Ms]**	**k_{off} [1/s]**
Spot 1(= 4900 RU)	443	382	1.6	0.0599	404	359	1.7	0.0609
Spot 2(= 4800 RU)	477	416	1.6	0.0649	444	388	1.7	0.0657
Spot 1 (=4500 RU)	585	508	1.3	0.0665	n.d.	n.d.	n.d.	n.d.
Spot 2 (=4500 RU)	510	438	1.4	0.0602	414	394	1.5	0.0603
Mean	503	436	1.5	0.0629	421	380	1.6	0.0623
Standard Deviation	61	53	0.1	0.0034	21	19	0.1	0.0030

Table S2. Results for the measurements of **5** with two different degrees of purity. The results are very similar in both cases.

Ligand	**4-CBS**				**sulfanilamide**			
	K_D (st-st) [µM]	**K_D (kin) [µM]**	**k_{on} [x 10^4 1/Ms]**	**k_{off} [1/s]**	**K_D (st-st) [µM]**	**K_D (kin) [µM]**	**k_{on} [x 10^4 1/Ms]**	**k_{off} [1/s]**
Spot 1(= 4900 RU)	0.99	0.89	6.5	0.0579	6.17	5.23	3.9	0.2023
Spot 2(= 4800 RU)	0.92	0.95	6.4	0.0605	7.17	5.82	3.7	0.2147
Spot 1 (=4500 RU)	1.01	0.90	6.2	0.0557	6.21	5.38	3.6	0.1963
Spot 2 (=4500 RU)	0.96	0.82	6.8	0.0559	6.24	5.77	3.6	0.2080
Mean	0.97	0.89	6.5	0.0575	6.45	5.55	3.7	0.2053
Standard Deviation	0.04	0.05	0.3	0.0022	0.48	0.29	0.1	0.0079
Literature (bCAII) *	n.d.	0.89	4.1	0.0369	n.d.	5.88	2.3	0.1330

Table S3. Validation of the SPR measurements of the compounds 4-CBS (**6**) and sulfanilamide (**7**) with hCAII against reference results. Results for the measurements of the reference compounds **6** and **7** with hCAII and comparison with literature data for bCAII from reference.[22] Abbreviations st-st and kin stand for steady-state and kinetic, respectively.

With 0.05 % Tween 20:								
Spot 1 (=3700 RU)					Spot 2 (=3600 RU)			
	K_D(st-st) [µM]	**K_D (kin) [µM]**	**k_{on} [x 10^5 1/Ms]**	**k_{off} [1/s]**	**K_D (st-st) [µM]**	**K_D (kin) [µM]**	**k_{on} [x 10^5 1/Ms]**	**k_{off} [1/s]**
1	1002.0	1073.4	1.6	0.1696	1037.0	1183.9	1.5	0.1828
2	382.2	318.8	1.9	0.0617	429.8	333.5	2.0	0.0664
3	133.7	91.4	5.1	0.0464	157.3	93.8	5.4	0.0504
4	63.4	57.4	8.7	0.0498	66.8	64.5	9.6	0.0617
5	452.8	418.3	1.6	0.0673	488.6	448.0	1.7	0.0741
Without Tween 20:								
Spot 1 (=3700 RU)					Spot 2 (=3600RU)			
	K_D(st-st) [µM]	**K_D (kin) [µM]**	**k_{on} [x 10^5 1/Ms]**	**k_{off} [1/s]**	**K_D (st-st) [µM]**	**K_D (kin) [µM]**	**k_{on} [x 10^5 1/Ms]**	**k_{off} [1/s]**
1	n.d.	n.d.	n.d.	n.d.	n.d.	n.d.	n.d.	n.d.
2	292.3	265.9	2.1	0.0554	312.2	277.0	2.0	0.0547
3	122.0	107.1	4.5	0.0483	126.4	113.2	4.6	0.0523
4	66.1	60.5	7.8	0.0472	66.1	62.8	8.4	0.0528
5	412.8	386.1	1.5	0.0596	425.2	402.2	1.7	0.0667

Table S4. Effects of Tween 20 addition to the running buffer. The same series of measurements was performed two times on the same protein surface. One time 0.05% Tween 20 was added to the running buffer and one time omitted. Similar values were obtained in both cases.

	Complex				
	hCAII-**1**	hCAII-**2**	hCAII-**3**	hCAII-**4**	hCAII-**5**
PDB entry	**4YX4**	**4YXI**	**4YXO**	**4YXU**	**4YYT**
Data collection and processing					
Wavelength [Å]	0.91841	0.91841	0.91841	0.91841	0.91841
Space group	$P2_1$	$P2_1$	$P2_1$	$P2_1$	$P2_1$
Unit cell parameters					
a,b,c [Å]	42.4, 41.5, 72.3	42.5, 41.5, 72.5	42.4, 41.6, 72.3	42.3, 41.7, 72.2	42.5, 41.7, 72.3
α,β,γ [°]	90, 104.4, 90	90, 104.5, 90	90, 104.3, 90	90, 104.3, 90	90, 104.3, 90
Matthews coefficient [$Å^3$/Da] *1	2.1	2.1	2.1	2.1	2.1
Solvent content [%]	40.6	40.9	40.8	40.8	41.0
Diffraction data					
Resolution range [Å]	35.70- 1.01 (1.07- 1.01)	41.11- 0.96 (1.02- 0.96)	35.05 – 1.06 (1.12 – 1.06)	41.44- 1.08 (1.15- 1.08)	41.14- 1-07 (1.13-1.07)
Unique reflections	126327 (19756)	148298 (23592)	108590 (17145)	103099 (16077)	107591 (17203)
R(I)sym [%]	4.9 (41.9)	4.4 (38.4)	7.7 (49.0)	5.5 (38.6)	5.8 (49.1)
Completeness [%]	98.7 (96.0)	99.2 (98.1)	98.0 (96.3)	98.0 (95.0)	99.3 (98.9)
Redundancy	3.2 (2.8)	3.5 (3.2)	3.6 (3.6)	3.3 (3.2)	3.2 (3.0)
I/σ(I)	11.0 (2.0)	13.3 (2.4)	9.1 (2.1)	12.1 (2.6)	11.6 (2.1)
Refinement					
Resolution range [Å]	35.70- 1.01	41.11- 0.96	35.05 – 1.06	41.44- 1.08	41.44- 1.08
Reflections used in refinement (work/free)	126327 (120010/6317)	148294 (140879/7415)	108590 (103160/5430)	103099 (97944/5155)	107591 (102211/5380)
Final R values for all reflections (work/free) [%]	15.1/.17.0	14.0/ 15.3	14.9/ 16.4	14.4/ 16.3	14.4/ 16.6
Protein residues	257	257	257	258	257
Atoms $1^{st}/2^{nd}/3^{rd}/4^{th}$ Inhibitor	10/-/-/-	11/11/-/-	12/12/-/-	13/13/-/-	13/13/13/11
Water molecules	249	258	235	244	245

RMSDs from ideality *2					
Bonds lengths[Å]	0.005	0.005	0.005	0.005	0.005
Bond angles [°]	1.1	1.1	1.1	1.1	1.1
Ramachandran plot *3					
Residues in most favored regions [%]	88.4	88.9	89.4	88.9	88.9
Residues in additional allowed regions [%]	11.1	10.6	10.2	10.6	10.6
Residues in generously allowed regions [%]	0.5	0.5	0.5	0.5	0.5
Mean B-factor [Å] *4					
Protein	12.6	10.7	12.5	10.4	10.4
$1^{st}/2^{nd}/3^{rd}/4^{th}$ Inhibitor	10.7/-/-/-	8.4/16.1/-/-	11.1/19.1/-/-	9.5/14.6/-/-	8.3/13.6/19.0/ 17.4
Water molecules	27.0	25.0	26.6	24.0	24.5

Table S5. Data collection and refinement statistics for the complex structure of 1-5.*1 Matthews coefficients were calculated according to literature.[14-16] *2 calculated with MolProbity[17] as implemented in the Phenix-suite.[23] *3 Ramachandran plots were generated with PROCHECK.[18] *4 Mean *B* factors were generated with MOLEMAN.[19] Numbers in brackets are for the highest resolution shell.

SECTION E. MISCELLANEOUS.

Crystallographic Water Structure.

We collected the structural data using 25 % (V/V) glycerol which is routinely used as a cryoprotectant for hCAII crystals. Aggarwal et al. showed that glycerol is able to displace three water molecules.[20] An overlay of our hCAII-**1** complex structure with a high resolution *apo*-structure of hCAII (pdb: 3KS3,[13] 0.90 Å) shows a similar finding (Figure S5c). The waters shown as blue- and as red-colored spheres were found in the *apo*-structure, those waters shown as green colored spheres belong to the hCAII-**1** structure. In the hCAII-**1** structure the glycerol displaces the three water molecules shown in blue which are detected in the *apo*-structure. Interestingly, waters W2-W5 of the hCAII-**1** complex are found in equal position in the *apo*-structure. So we estimate that the glycerol molecule does not influence the water structure significantly. The waters W2-W6 are found in very similar positions for ligands **1**-**5** (Figure 4 and Figure S4). For ligands **1**-**4** the Lee-Richard surfaces are shown. The Lee-Richard surface is an estimation of the solvent accessible surface area (SASA).[21] All detected waters coincide or fall close to the surface of this SASA. W1 is present in the complexes hCAII-**2**-**5** at virtually the same position. In the hCAII-**1** structure it can penetrate deeper into the pocket since **1** does not possess a hydrophobic tail pushing W1 to the position which it occupies in hCAII-**2**-**5**. In hCAII-**1**W1 constructs an H-bond network with waters W7 and W8. Water W7 is only present in the hCAII-**1** structure because only here it can be stabilized by an H-bond with W1. Furthermore, in hCAII-**2**-**4** it will be displaced owing to the steric requirements of the hydrophobic tail of the ligand. Only for **1** the position of W7 falls outside the Lee-Richard surface around the ligand. W8 is also visible in the hCAII-**3** and hCAII-**5** structures. In hCAII-**2** some F_o-F_c difference electron density (3.13 σ, 0.50 e/Å^3) could be detected at the position for W8 (Figure S4a) but its shape and magnitude did not fully justify the placement of a full water molecule in the refinement. However, W8 seems to be stabilized in the hCAII-**2** complex, but not to

the same extent as in hCAII-**1**, hCAII-**3** and hCAII-**5**. A density peak suggests occupancy of W8 in hCAII-**3,** however, without being connected to the remaining active site water molecules (Figure S4b). An additional water (W11) is visible in the hCAII-**3** structure. It lies above W1 and W3 and is stabilized by H-bonds to the latter water molecules. Both W8 (3.4 Å) and W11 (4.0 Å) are stabilized by a van der Waals contact to the terminal methyl group of **3**. Similar contacts are visible between the ethyl group of **2** to W1 (3.6 Å) and the terminal methyl group of **4** to W1 (3.5 Å). In hCAII-**4** no evidence for the presence of W8 could be detected. This is in good agreement with the Lee-Richard surface (main text Figure 4b) which extends as a consequence of the additional carbon atom of **4** into the region being occupied by W8 in hCAII-**1**, -**3** and -**5**. The terminal hydroxyethylene group of **5** is visible in two orientations. The higher populated orientation A (58 %) forms an H-bond with the glycerol molecule while the orientation B (42 %) is similarly orientated as the tail of **4**. In orientation B the terminal OH group of **5** forms H-bonds to the neighboring water molecules W1 and W8. We assume that orientation B is the predominant one in the glycerol-free condition since the described H-bond between the terminal OH group of the tail of **5** in the orientation A to the glycerol could not be established. Orientation A will exclude presence of W3 as the OH group of **5** (1.7 Å) would come very close. Accordingly, W3 is only present when **5** is in orientation B. Ligand **1** is the only one which is bordered by a contiguously connected water structure on the side towards the solvent. This ligand shows a significantly faster dissociation as **2-5**. Based on the crystallographic analysis the deviating water structure is the most striking difference of **1** compared to **2-5**, thus possibly the better established water network favors the faster dissociation of **1** since the ligand might be more easily displaced by water molecules. However, as these changes occur at the already solvent-exposed face of the ligands it remains unclear how strongly the water structure influences the dissociation velocity. For the complex structures of ligands **2-5** additional molecules of the respective ligand could be found in the F_o-F_c difference electron densities. For **2-4** one additional ligand, for ligand **5** three additional ligands could be placed. Crystal packing effects together with the high concentrations of the ligands applied in the

soaking buffer might be responsible for this observation. The additional binding position observed for **5** adjacent to the active site (Figure S6b and Figure S6c) might suggest a putative position intermediately occupied by the ligands before they slip into the final binding position in the active site. This additional binding mode was only observed for **5**. Further investigation is needed to fully unravel the significance of this mode at lower ligand concentrations, since no conformations of this type was observed during MD simulations of one single fully solvated ligand-protein complex. Due to the additional polar group **5** shows a higher solubility than all other compounds. This might explain why we find only for this ligand three additional molecules in the F_o-F_c difference electron density since saturated solutions of the ligands were applied. The terminal hydroxyethylene tail of this extra molecule of **5** could only be modeled up to the first carbon atom since the remaining atoms are not unambiguously defined in the difference electron density. Figure S6 shows the surface of the next symmetry mate in the crystal packing (colored in blue). It contributes to the stabilization of the binding mode of this additional ligand since it forms a cavity with the neighboring protein molecule (colored in gray). Apart from the contact to the crystal mate also interactions to residues of the same protein molecule are formed thus suggesting that also the binding in solution could be established (Figure S6b and Figure S6c). The nitrogen of the additional molecule of **5** forms an H-bond to one of the oxygens of the carboxylic acid group of Glu 69 (2.7 Å) while one of its oxygen atoms forms an H-bond with the carboxamide nitrogen of Asn 67 (3.1 Å). Van der Waals interactions between the aromatic ring (4.1 Å) and the first carbon atom of the tail of **5** (4.5 Å) to the side chain of Ile 91 are detected. Since this residue is part of the hydrophobic patch, it could be envisaged that this pose, similarly to the ones located at the secondary patch, is also stabilized by favorable hydrophobic interactions.

Rate equations.

In the pre-equilibration hypothesis the unbound system is taken to be in equilibrium with the F basin and yields:

$$k_1[P][L] = k_{-1}[F] \qquad (3)$$

We now work under the hypothesis that the variation of [S] during the reaction is small enough for steady state kinetics to be applied:

$$k_2[F] - k_{-2}[S] - k_3[S] = \frac{\partial[S]}{\partial t} = 0 \qquad (4)$$

The rate of formation of the bound state at the last association step is:

$$k_3[S] = \frac{\partial[PL]}{\partial t} \qquad (5)$$

Combining equation (3) and (4) it is possible to express [S] in terms of the unbound state concentration [P][L]. Plugging the expression into (3) we get:

$$\frac{k_1}{k_{-1}}\frac{k_2 k_3}{k_{-2} + k_3}[P][L] = \frac{\partial[PL]}{\partial t} = k_{on}[P][L] \qquad (6)$$

SECTION F. REFERENCES.

(1) Hellriegel, C.; Rueck, A. Practical Aspects in Quantitative NMR. Technical Details for the Purity Determination of Organic Substances. *Sigma Aldrich Analytix* 1/**2015**, 6-8

(2) Pauli, G. F.; Chen, S.-N.; Simmler, C.; Lankin, D. C.; Gödecke, T.; Jaki, B. U.; Friesen, J. B.; McAlpine, J. B.; Napolitano, J. G. Importance of Purity Evaluation and the Potential of Quantitative ^{1}H NMR as a Purity Assay. *J. Med. Chem.* **2014**, 57 (22), 9220

(3) Zheng, Y.; Liu, B.; Gou, Z.; Li, Y.; Zhang, X.; Wang, Y.; Yu, S.; Li, Y.; Sun, D. Design of novel CSA analogues as potential safeners and fungicides. *Bioorg. Med. Chem. Lett.* **2015**, 25 (4), 791

(4) Chern, J.-W.; Leu, Y.-L.; Wang, S.-S.; Jou, R.; Lee, C.-F.; Tsou, P.-C.; Hsu, S.-C.; Liaw, Y.-C.; Lin, H.-M. Synthesis and Cytotoxic Evaluation of Substituted Sulfonyl-*N*-hydroxyguanidine Derivatives as Potential Antitumor Agents. *J. Med. Chem.* **1997**, 40 **(**14), 2276

(5) Moriyama, K.; Nakamura, Y.; Togo, H.; Oxidative Debenzylation of *N*-Benzyl Amides and *O*-Benzyl Ethers Using Alkali Metal Bromide. *Org. Lett.* **2014**, 16 (14), 3812,

(6) Sun, H.-X.; Sun, Z.-H.; Wang, B. *B*-Alkyl Suzuki–Miyaura cross-coupling of tri-*n*-alkylboranes with arylbromides bearing acidic functions under mild non-aqueous conditions. *Tetrahedron Lett.* **2009**, 50 (14), 1596

(7) Imamura, Y.; Higuchi, T.; Otagiri, M.; Nagumo, S.; Akita, H. Catalytic Properties of Carbonyl Reductase from Rabbit Kidney for Acetohexamide and Its Analogs. *Bioorg. Chem.* **1994**, 22 (4), 387

(8) van Es, T.; Backeberg, O. G.; Morrison, I. Some sulfonamido derivatives of stilbene and acetophenone. *J. S. Afr. Chem. Inst.* **1964**, 17 (2), 95

(9) Feichtinger, H. Notiz über die Willgerodt-Reaktion von 1^{1}-Chlor-toluol-sulfonsäure-(4)- und -(2)-chlorid. *Chem. Ber.* **1971**, 104 (5), 1697

(10) Benedetti, P. G. de; Iarossi, D.; Menziani, M. C.; Frassineti, C.; Benedetti, A. Multinuclear NMR and vibrational spectroscopy studies of the substituent effects in benzensulphonamide inhibitors of the enzyme carbonic anhydrase. *J. Mol. Struct.* **1988**, 175, 37

(11) Shil, A. K.; Sharma, D.; Guha, N. R.; Das, P. Solid supported Pd(0): an efficient recyclable heterogeneous catalyst for chemoselective reduction of nitroarenes. *Tetrahedron Lett.* **2012**, 53 (36), 4858

(12) Scott, A. D.; Phillips, C.; Alex, A.; Flocco, M.; Bent, A.; Randall, A.; O'Brien, R.; Damian, L.; Jones, L. H. Thermodynamic optimization in drug discovery: a case study using carbonic anhydrase inhibitors. *ChemMedChem* **2009**, 4, 1985−9.

(13) Avvaru, B. S.; Kim, C. U.; Sippel, K. H.; Gruner, S. M.; Agbandje-McKenna, M.; Silverman, D. N.; McKenna, R. A short, strong hydrogen bond in the active site of Human Carbonic Anhydrase II. *Biochemistry* **2010**, 49, 249.

(14) Matthews, B. W. Solvent content of protein crystals. *J. Mol. Biol.* **1968**, 33, 491.

(15) Kantardjieff, K. A.; Rupp, B. Matthews coefficient probabilities: Improved estimates for unit cell contents of proteins, DNA, and protein–nucleic acid complex crystals**.** *Protein Sci.* **2003**, 12, 1865.

(16) Weichenberger, C. X.; Rupp, B. Ten years of probabilistic estimates of biocrystal solvent content: new insights *via* nonparametric kernel density estimate. *Acta Crystallogr. Sect. D: Biol. Crystallogr.* **2014**, 70, 1579.

(17) Chen, V. B.; Arendall, W. B., 3rd; Headd, J. J.; Keedy, D. A.; Immormino, R. M.; Kapral, G. J.; Murray, L. W.; Richardson, J. S.; Richardson, D. C. MolProbity: all-atom structure validation for macromolecular crystallography. *Acta crystallogr. Sect. D: Biol. Crystallogr.* **2010**, 66, 12.

(18) R. A. Laskowski, M. W. M., D. S. Moss, J. M. Thornton. PROCHECK: A program to check the stereochemical quality of protein structures. *J. Appl. Crystallogr.* **1993**, *26*, 283.

(19) G.J. Kleywegt, J.-Y. Z., M. Kjeldgaard, T.A. Jones in *Int. Tables Crystallogr.*; M. G. Rossman, E. A., Ed. Netherlands, Dordrecht, 2001; Vol. F, p 353.

(20) Aggarwal, M.; Boone, C. D.; Kondeti, B.; Tu, C.; Silverman, D. N.; McKenna, R. Effects of cryoprotectants on the structure and thermostability of the human carbonic anhydrase II–acetazolamide complex. *Acta Crystallogr. Sect. D: Biol. Crystallogr.* **2013**, *69*, 860.

(21) Lee, B.; Richards, F. M. The interpretation of protein structures: estimation of static accessibility. *J. Mol. Biol.* **1971**, *55*, 379.

(22) Myszka, D. G. Analysis of small-molecule interactions using Biacore S51 technology. *Anal. Biochem*. **2004**, 329, 316−323.

(23) Adams, P. D.; Afonine, P. V.; Bunkoczi, G.; Chen, V. B.; Davis, I. W.; Echols, N.; Headd, J. J.; Hung, L.-W.; Kapral, G. J.; Grosse-Kunstleve, R. W.; McCoy, A. J.; Moriarty, N. W.; Oeffner, R.; Read, R. J.; Richardson, D. C.; Richardson, J. S.; Terwilliger, T. C.; Zwart, P. H. PHENIX: a comprehensive Python-based system for macromolecular structure solution. *Acta Crystallogr., Sect. D: Biol. Crystallogr.* **2010**, *66*, 213−221.